PERGAMON

Vacuum 63 (2001) 307–313

VACUUM
SURFACE ENGINEERING, SURFACE INSTRUMENTATION & VACUUM TECHNOLOGY

www.elsevier.nl/locate/vacuum

Phase decomposition in polymer blend films cast on substrates patterned with self-assembled monolayers

P. Cyganik[a], A. Bernasik[b], A. Budkowski[a,*], B. Bergues[a], K. Kowalski[b], J. Rysz[a], J. Lekki[c], M. Lekka[c], Z. Postawa[a]

[a]*Smoluchowski Institute of Physics, Jagellonian University, Reymonta 4, 30-059 Kraków, Poland*
[b]*Surface Spectroscopy Laboratory, University of Mining and Metallurgy and Joint Centre for Chemical Analysis and Structural Research, Jagellonian University, Kraków, Poland*
[c]*Institute of Nuclear Physics, Radzikowskiego 152, Kraków, Poland*

Abstract

Thin polymer films with lateral structures are expected to play an important role in future applications (e.g. plastic-based electronic devices). Such structures could be formed when blend films are spun-cast onto substrates patterned with self-assembled monolayers (SAM). The spin-coating process results in composition variations accompanied by surface undulations. We have studied both phenomena for PVP/dPS and PVP/PBrS blends, composed of poly(vinylpyridine) (PVP) and deuterated (dPS)- or brominated (PBrS)-polystyrene. SAM stripes of $HS(CH_2)_{15}CH_3$ on Au substrate ('bare' or covered with $HS(CH_2)_{15}COOH$) were used as the pattern with periodicity of 4 μm. Transfer of the pattern from the substrate to the film interior and to the film surface was examined with secondary ion mass spectroscopy (SIMS) and atomic force microscopy (AFM) combined with selective dissolution of blend components. Characteristic size D of the phase domains corresponding to given spin-casting conditions was determined for the blends cast on homogeneous SAM substrate. Fourier transform analysis (FTA) of topographic (AFM) and compositional (SIMS) maps was performed. FTA confirms that the pattern-directed composition variations coincide with the surface undulations. It reveals also that most effective pattern transfer is achieved for the size D commensurate with the pattern periodicity for the carefully adjusted polymer–substrate interactions.

Keywords: Phase separation morphology; Thin films; Polymer blends; Self-assembled monolayers; Atomic force microscopy; Secondary ion mass spectroscopy

1. Introduction

External surfaces can significantly alter the phase decomposition (PD) of polymer blends in thin films [1]. The break of the symmetry of polymer mixture and preferential attraction of one of the blend components lead to an surface-oriented mode of PD [1–4] or the formation of wetting layers [5–7]. A controlled variation of the interactions between polymers and *homogeneous* surfaces has been recently accomplished for both, air/polymer and polymer/substrate interfaces [3,8,9]. It has been demonstrated that modified aggregation of blend phases at external surfaces results in different

* Corresponding author. Fax: + 48-12-633-7086.
E-mail address: ufbudkow@cyf-kr.edu.pl (A. Budkowski).

0042-207X/01/$ - see front matter
PII: S0042-207X(01)00206-8

morphologies of phase domain structures [7,10]. The lateral modification of the polymer–surface interactions is feasible only for pre-structured substrates. Various methods can be used to produce periodic patterns of chemically *heterogeneous* substrates [11–16]. The most versatile is micro-contact printing [12–14,16]. This soft-lithographic procedure covers metal substrate with patterns of self-assembled monolayers (SAM). The alignment of blend phases with respect to the patterned substrate has been observed in thin films for the mixtures quenched outside one-phase region of the phase diagram [11–15]. In those studies molecular mobility was promoted by elevated temperature (*temperature quench* [11,12,14]) or by a common solvent added to the polymer blend (*solvent quench* [13,15]). The self-ordering of blend phases due to the transfer of the substrate pattern can be employed in new polymer-based technologies of photo-electronic devices or microelectronic circuits [17].

Substrate pattern-oriented PD can be reflected in deformations of the flexible air/film interface. Surface undulations are driven by the modulation of surface tension (temperature quench) [12,14] or the variation of solvent evaporation rate (solvent quench) [13] from one blend phase to the other. While same overall coincidence between phase domain morphology and surface topography has been concluded from the results of atomic force microscopy (AFM) combined with selective dissolution of blend phases [13], their exact correspondence has been so far only assumed [12,14]. The application of imaging secondary ion mass spectroscopy (SIMS) [18] has enabled us to present in this paper the first exact reconstruction of the true three-dimensional phase domain structure in polymer blend films on patterned substrate. We examine with Fourier transform analysis (FTA) the composition (SIMS) and topographic (AFM) maps and confirm their correspondence.

We also discuss the efficiency of the pattern transfer from the substrate to blend films for the solvent quench. We consider the following parameters controlling this process: (a) the ratio D/λ of characteristic phase domain size D and pattern periodicity λ; (b) the polymer–surface interactions. In contrast to previous studies [13,15] FTA is applied and more systematic analysis of one system and its modifications (to vary the solvent quench parameters we have exchanged one of two polymer blend components or one of two alternating stripes forming the patterned substrate) is presented.

2. Experimental

The PVP/dPS and PVP/PBrS blends composed of poly(vinylpyridine) (PVP) and deuterated polystyrene (dPS) or partially brominated polystrene (PBrS, with 10.5% segments brominated) were investigated. Characteristics of polymers used are presented in Table 1. In our experiments phase decomposition due to the solvent quench takes place during the spin-casting procedure. In the first step two polymer blend components with fixed 50% PVP mass fraction were dissolved in a common solvent (tetrahydrofurane, THF). Then a drop of the solution was placed on a substrate, and thin films were prepared through a rapid rotation of the substrate. The combination of total polymer concentration (10.7–14 mg/ml) and spin speed (ca.

Table 1
Characteristics of the polymers (molecular weight M_w, polydisperisty M_w/M_n, solubility parameter δ) and solvents used in the present study

Polymer	M_w (M_w/M_n)	δ [(MPa)$^{1/2}$]	Solvent	δ [(MPa)$^{1/2}$]
Deuterated polystyrene (dPS)	174 k (1.03)	18.7[a]	Tetrahydrofurane (THF)	18.2[a]
Partially brominated polystyryne (PBrS)	171 k (1.04)	~ 18.9[b]	Ethanol	25.4[a]
Poly(vinylpyridine) (PVP)	115 k (1.02)	~ 20.6[b]		

[a]Ref. [20].
[b]Evaluated using interaction parameter data [7,19].

5800 rpm) resulted in films with nominal (i.e. average) thickness $d \sim 50$–80 nm.

Patterned heterogeneous substrates (SAM_0/Au and SAM_0/SAM_1) used consist of alternating (with the periodicity $\lambda = 4\,\mu m$) 2 μm-wide stripes composed of: bare gold (Au), gold surface covered with hydrophobic (SAM_0) and with hydrophilic (SAM_1) SAM monolayers. Characteristics of these substrates are presented in Table 2. Micro-contact printing procedure [16] was used to create SAM_0 stripes. A patterned elastomer stamp printed the 'ink' of $HS(CH_2)_{15}CH_3$ molecules in 10 mM ethanol solution onto Au surface. To produce the SAM_0/SAM_1 surfaces the printed SAM_0/Au substrates were immersed additionally in 10 mM ethanol solution of $HS(CH_2)_{15}COOH$ [12,14]. In addition, homogeneous Au and SAM_0 substrates were used to evaluate the phase domain morphology and its characteristic size D corresponding to given spin-casting conditions.

Phase domain morphology was studied with two SIMS techniques and one AFM-related procedure. Depth profiling SIMS [3–6,18] reveals the average concentration ϕ of blend components as a function of distance z from the air/film interface. Imaging SIMS [18] reproduces true three-dimensional chemical composition in the form of $\phi(x, y)$-images for the successively excavated layers. Depth profiling (with resolution better than 6 nm half width at half maximum) and imaging SIMS (with Rayleigh lateral resolution of ca. 120 nm) data were obtained with VSW apparatus equipped with a double lens liquid metal ion gun (Fei Company) and with a quadrupole mass spectrometer (Balzers) with a cylindrical mirror energy filter at the entrance [18]. The overall phase domain morphology was determined by AFM (Park Scientific Instruments) examination combined with selective dissolution of PVP-rich phase for films immersed in ethanol [13]. AFM was used also to study the topography of surface undulations.

Table 2
Static water contact angle Θ of substrate surfaces: bare Au and Au surface covered with self-assembled monolayers: $HS(CH_2)_{15}CH_3$ (SAM_0) and $HS(CH_2)_{15}COOH$ (SAM_1)

Substrate	Θ (deg)
SAM_0	108[a]
Au	65[a]
SAM_1	< 10[b]

[a]Ref. [21].
[b]Ref. [22].

3. Results

We begin this section with the description of the pattern-directed phase decomposition (PD) in the PVP/PBrS blend films on the SAM_0/Au substrate. Then we consider the results for the PVP/dPS films coating the SAM_0/Au and SAM_0/SAM_1 substrates. To understand PD in PVP/PBrS cast on the heterogeneous substrate SAM_0/Au it is instructive to discuss first PD taking place for the same blend on homogeneous SAM_0 and Au surfaces. Phase domain morphology can be deduced from AFM and SIMS data shown in Fig. 1. A bilayer composed of PBrS- and PVP-rich laminated domains adjacent to (smooth) air and substrate interfaces, respectively, is observed for PVP/PBrS blend cast on Au (Figs. 1a and b). The PVP/PBrS interface (characterised by the width [7] $w = 10$ nm) is much wider than that expected ($w = 1.2$ nm) for these incompatible polymers in thermodynamic equilibrium [7,10,20]. Drastically changed morphology is observed for the PVP/PBrS blend coating the SAM_0 substrate. Corrugated film surface topography (Fig. 1c) with vertical distance amplitude $\Delta h \approx 26$ nm and different for both phases effective thickness (approximated very roughly by the range Δz of the distance z from the air interface $\Delta z(\mathrm{PVP}) \sim 75$ nm and $\Delta z(\mathrm{PBrS}) \sim 53$ nm (see Fig. 1d) suggests a formation of laterally disordered phase domains, which are higher and more narrow for PVP than for PBrS. These results indicate that more polar PVP is favoured at the Au surface, while no preferential attraction takes place for the SAM_0 substrate.

Now we are ready to discuss PD in the PVP/PBrS blend film cast on the heterogeneous substrate SAM_0/Au at the conditions identical to those used for homogenous surfaces (Fig. 1). AFM images (Figs. 2a and b) show relatively good ordering of surface undulations, resembling the substrate pattern. Narrow and elevated strips alternate with

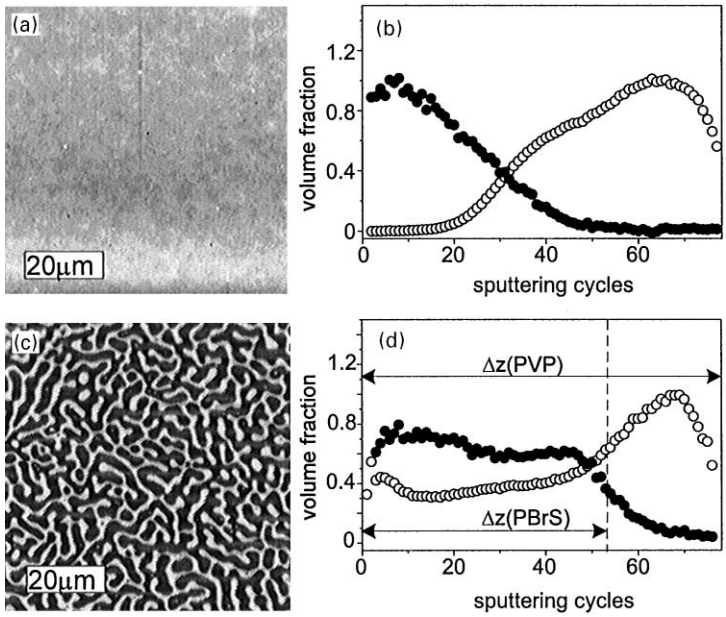

Fig. 1. AFM images (a, c) of the air/film interface and SIMS depth profiles (b, d) of the PVP/PBrS blend film cast on homogeneous Au (a, b) and SAM_0 (c, d) substrates. Vertical distance (peak to valley) amplitude $\Delta h \approx 1$ nm in (a) and 26 nm in (c). Depth SIMS profiles of the average chemical composition ϕ vs. the distance from the air surface (1 sputtering cycle ≈ 1 nm) corresponding to both blend components: PVP (open circles) and PBrS (solid circles).

wider regions located lower. The results shown in Fig. 1 suggest that the linear protrusions correspond to the phase rich in PVP. This structural feature is confirmed by AFM image (Fig. 2d), which was taken after selective dissolution of the PVP-rich phase domains. The overall morphology concluded from our measurements is presented in Fig. 2c. We postulate that protruded linear PVP domains are located on Au stripes, while PBrS-rich phase is displaced onto SAM_0 substrate regions with no preferential attraction.

To examine more quantitatively topographic and compositional maps we have analysed their two-dimensional fast Fourier transforms (FFT). Radial averages of the squared FFT amplitudes were used to calculate power spectra $P_i(k)$ corresponding to *isotropic* maps of the blends cast on homogeneous substrates. FFT spectra for the blends on patterned substrates exhibit isotropic (diffusive ring) and *anisotropic* (series of sharp peaks distributed along one line) components. The latter were used to compute power spectra $P_a(k)$ analysed later. Typical distributions $P_i(k)$ and $P_a(k)$, corresponding to Figs. 1c and 2a are presented in Figs. 2f and e, respectively. Spectra $P_i(k)$ have maximum at the wave vector $k = 1/D$ allowing us to determine the average domain size D. For the PVP/PBrS blend films presented in Figs. 1–2 the calculated value of $D = 3.9(1)\,\mu$m matches the substrate pattern periodicity ($\lambda = 4\,\mu$m). The corresponding power spectrum $P_a(k)$ of this blend on the patterned SAM_0/Au substrate (Fig. 2e) exhibits distinct maximums at $k = 1/\lambda$ and $2/\lambda$. Higher harmonics n/λ ($n > 1$) have not been observed for temperature quenched films with $D = \lambda$ [12,14]. We postulate that they may appear here due to very rapid blend solidification in the spin-casting process [13].

To examine the role of the blend components we have studied films cast in conditions identical to those described above but with PBrS exchanged by dPS. The domain size $D = 4.1(1)\,\mu$m for PVP/dPS accords with $D = 3.9(1)\,\mu$m determined for PVP/PBrS (cf. Fig. 3a and 1c). This is related to almost unaffected compatibility of blend

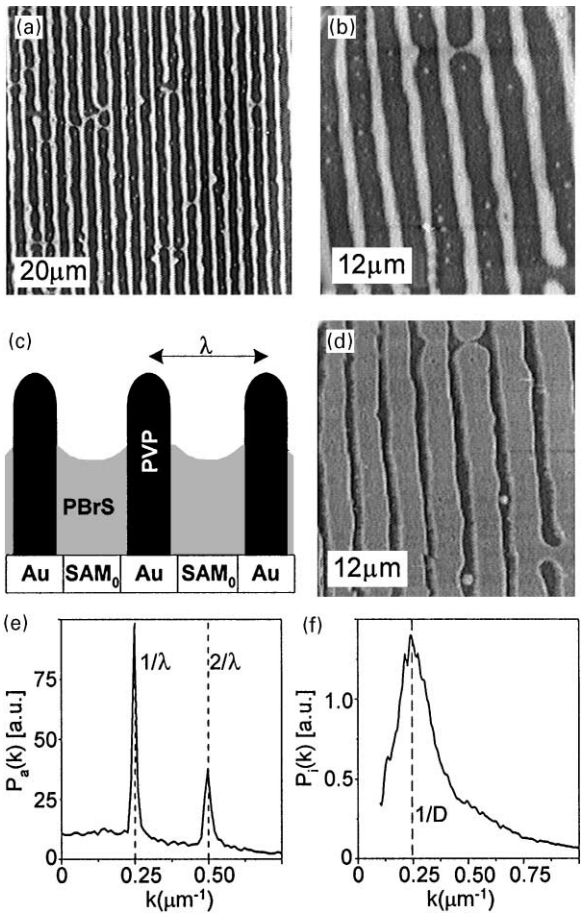

Fig. 2. (a), (b) and (d) AFM images of the PVP/PBrS blend films on the SAM_0/Au substrate: (a, b) as cast (the same casting conditions as for Fig. 1, $\Delta h \approx 29$ nm); (d) after immersion for 5 min in ethanol (selective solvent for PVP, $\Delta h \approx 40$ nm) on the same spot as in (b); (c) the overall phase domain morphology; (e)–(f) power spectra obtained from anisotropic and isotropic (radial averaged) components of fast Fourier transforms (FFT) corresponding to Figs. 2a (e) and 1c (f), respectively. Characteristic average phase domain size $D = 3.9(1)\,\mu$m.

components (the solubility parameters δ of PBrS and dPS are very similar, see Table 1). Polymer exchange induces a better ordering of surface patterns. Linear protrusions sporadically connected for PVP/PBrS (Fig. 2a) are well separated for PVP/dPS (Fig. 3b). We attribute this improvement to increased difference in the interactions of blend constituents with Au stripe of the SAM_0/Au substrate (Au may slightly attract polar PBrS but not dPS).

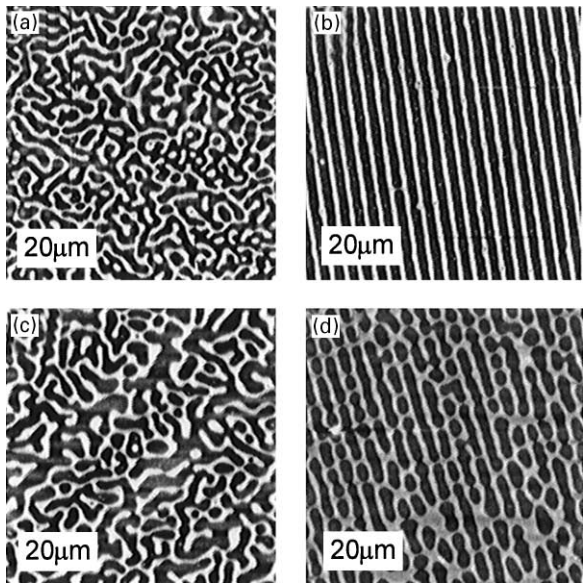

Fig. 3. (a)–(d) AFM images ($\Delta h \approx 26$, 33, 30, 40 nm for (a–d), respectively) of the PVP/dPS blend films on the SAM_0 (a, c) and SAM_0/Au substrates (b, d). Average phase domain size $D = 4.1(1)\,\mu$m (a,b) and $D = 5.3(1)\,\mu$m (c, d) determined from FFT of (a) and (c), respectively.

Now we consider how the pattern transfer from the substrate to the film is controlled by the characteristic domain size D. Previous studies [12–15] were focused on the regions $D \leqslant \lambda$ [12–14] and $D \gg \lambda$ [15]. Here we compare the results obtained for $D = \lambda$ (Fig. 3a–b) with data acquired for $D > \lambda$ (Figs. 3c and d). AFM images of the blend PVP/dPS cast on the SAM_0/Au substrate indicate drastic changes accompanying the modification of the domain size from $D = 4.1(1)\,\mu$m (Fig. 3b) to $D = 5.3(1)\,\mu$m (Fig. 3d), which was obtained by varying total polymer concentration in THF. Apparently too large phase domains (Fig. 3d) developing during the solvent quench are not very susceptible to periodic variations of substrate interactions. Optimum conditions (Fig. 3b) are achieved for the size D which commensurate with the periodicity λ.

In the discussion presented so far we have assumed the coincidence between surface topography and domain morphology suggested by the AFM results combined with selective dissolution proced-

ure (Fig. 2). A more careful examination of this problem is provided here by the SIMS reconstruction of three-dimensional phase domain structure. Figs. 4a–c present lateral PVP distribution maps recorded at various distances from the air surface of the PVP/dPS blend film on the SAM_0/Au substrate. AFM image of the unperturbed surface of this sample is shown in Fig. 3d. The comparison of both data types proves that the surface topographic features correspond directly to the overall phase domain morphology sketched in Fig. 2c (with PBrS exchanged by dPS). The coincidence between topography and morphology is confirmed also by FFT analysis (see Fig. 4d). Power spectrum $P_a(k)$ of the AFM image determined for the film *surface* topography (Fig. 3d, solid line in Fig. 4d) is in accordance with $P_a(k)$ of the PVP domain chemical (SIMS) map recorded for the region adjacent to the *substrate* (Fig. 4c, dashed line in Fig. 4d).

Finally, we demonstrate that the polymer-substrate interactions should be carefully adjusted to obtain effective transfer of the substrate pattern. The exchange of the SAM_0/Au for the SAM_0/SAM_1 heterogeneous substrate results in a larger surface energy difference between two types of alternating stripes (see the contact angle values presented in Table 2). Surprisingly this step does not improve but rather worsen the situation for the PVP/dPS blend films with the domain size $D \approx \lambda$ (cf. Figs. 3b and 5 for SAM_0/Au and SAM_0/SAM_1, respectively). Most probably the interactions (driving the lateral order in the film) between polar PVP and a dipole moment induced in Au are more favourable than those between PVP and the COOH-terminated SAM layer.

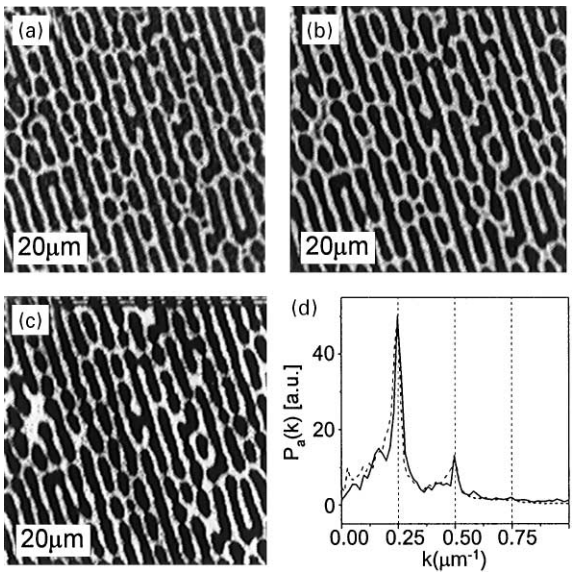

Fig. 4. (a)–(c) SIMS $\phi(x, y)$-images reconstructing the lateral distribution of PVP at the distance $z \approx 18$ nm (a), 55 nm (b) and 92 nm (c) from the air surface of the PVP/dPS blend film cast on the SAM_0/Au substrate. AFM image of the surface undulations (another spot) is shown in Fig. 3d. (d) Power spectra of anisotropic FFT of topographic (solid line, for Fig. 3d) and compositional (dashed line, for Fig. 4c) maps.

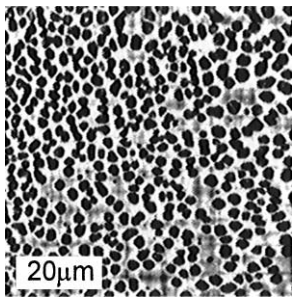

Fig. 5. AFM image ($\Delta h \approx 16$ nm) of the PVP/dPS blend film on the SAM_0/SAM_1 substrate. The same casting conditions were used as for Figs. 3a and b with the domain size $D = 4.1(1)$ μm.

4. Summary

We have studied different factors determining the phase domain morphology and surface topography of thin polymer films undergoing phase decomposition during spin coating onto patterned substrates. We have observed the transfer of the substrate pattern into film interior and film surface. Various experimental methods applied (especially imaging SIMS) allowed us to determine the real three-dimensional phase domain structure and to confirm the coincidence between the lateral structure of phase domains and the topography of surface undulations. We have focused our attention on the role of the polymer–substrate interactions and the optimal size of the phase domains.

Acknowledgements

This work was supported by Grants of the Institute of Physics, by Reserve of the Rector of the Jagellonian University, by Polish Committee of Scientific Research and by M. Sklodowska-Curie Foundation. One of us (J.R.) is grateful to the Foundation for Polish Science for financial support. The authors also thank Professor M. Szymoński for the access to AFM microscope at Regional Laboratory for Physical and Chemical Analysis of the Jagellonian University.

References

[1] Jones RAL, Norton LJ, Kramer EJ, Bates FS, Wiltzius P. Phys Rev Lett 1991;66:1326.
[2] Krausch G, Mater Sci Eng 1995;R14:1 and references therein.
[3] Rysz J, Bernasik A, Ermer H, Budkowski A, Brenn R, Hashimoto T, Jedliński J. Europhys Lett 1997;40:503.
[4] Rysz J, Ermer H, Budkowski A, Lekka M, Bernasik A, Wrobel S, Brenn R, Lekki J, Jedlinski J. Vacuum 1999;54:303.
[5] Rysz J, Budkowski J, Bernasik A, Klein J, Kowalski K, Jedliński J, Fetters LJ. Europhys Lett 2000;50:35.
[6] Rysz J, Budkowski A, Scheffold F, Klein J, Fetters LJ, Bernasik A, Kowalski K. Macromol Symp 2000;149: 277.
[7] Budkowski A, Adv Polym Sci 1999; 148: 1 and references therein.
[8] Genzer J, Kramer EJ. Phys Rev Lett 1997;78:4946.
[9] Mansky P, Liu Y, Huang E, Russell TP, Hawker C. Science 1997;275:1458.
[10] Binder K. Adv Polymer Sci 1999;138:1.
[11] Krausch G, Kramer EJ, Rafailovich MH, Sokolov J. Appl Phys Lett 1994;64:2655.
[12] Ermi BD, Nisato G, Douglas JF, Rogers JA, Karim A. Phys Rev Lett 1998;81:3900.
[13] Böltau M, Walheim S, Mlynek J, Krausch G, Steiner U. Nature 1998;391:877.
[14] Nisato G, Ermi BD, Douglas JF, Karim A. Macromolecules 1999;32:2356.
[15] Rockford L, Liu Y, Russell TP, Yoon M, Mochrie SGJ. Phys Rev Lett 1999;82:2602.
[16] Kumar A, Whitesides GM. Appl Phys Lett 1993;63:2002.
[17] Service RF. Science 1997;278:383.
[18] Bernasik A, Rysz J, Budkowski A, Kowalski K, Camra J, Jedliński J. 2000, submitted.
[19] Shull KR, Kramer EJ, Hadziioannou GH, Tang W. Macromolecules 1990;23:4780.
[20] Handbook of physical and chemical properties. Warsaw: WN-T, 1974 [in polish].
[21] Walheim S, Böltau M, Mlynek J, Krausch G, Steiner U. Macromolecules 1997;30:4995.
[22] Lee RT, Carey RI, Biebuyck HA, Whitesides GM. Langmuir 1994;10:741.